Intercomparison and Interpretation of Satellite-Derived Directional Albedos over Deserts

ROBERT D. CESS

Institute for Atmospheric Sciences, State University of New York, Stony Brook, New York

INNA L. VULIS*

Columbia University, New York, New York

(Manuscript received 8 April 1988, in final form 7 November 1988)

ABSTRACT

Desert regions are employed in somewhat of a tutorial mode for the purpose of addressing several issues associated with understanding the dependence of planetary (top-of-the-atmosphere) albedo upon solar zenith angle, i.e., the directional planetary albedo. It is emphasized that in evaluating this quantity from satellite data, and with reference to land surfaces, spurious results may be obtained if geographical variations of the planetary albedo are not isolated from the albedo's solar zenith angle dependence. An atmospheric solar radiation model is then coupled with desert surface bidirectional reflectance measurements to test for consistency with satellite-derived directional planetary albedos. The model is further used to address issues such as the use of narrowband versus broadband instruments, the impact of desert aerosols upon the directional planetary albedo, and to interpret potential differences in the directional planetary albedo associated with different types of deserts. The model results show consistency with satellite measurements, while further suggesting that over desert regions, narrowband instruments should replicate broadband measurements of the directional planetary albedo, as is also consistent with observations. The model shows that the directional planetary albedo is dominated by the directional surface albedo, although surface brightness is a second factor since it influences atmospheric limb brightening and limb darkening processes.

1. Introduction

Knowledge of the dependence of planetary (top-of-the-atmosphere) albedo upon solar zenith angle (i.e., directional planetary albedo), for different underlying surfaces, is necessary with respect to processing earth radiation budget data. In most instances, converting local-time albedos to diurnally-averaged quantities relies heavily upon the use of directional albedo models. Thus, the primary motivation for producing directional planetary albedos from Nimbus-7 data (Taylor and Stowe 1984, 1986) was to provide directional albedo models for use in processing Earth Radiation Budget Experiment (ERBE) data. Here, the surface types were categorized as ocean, desert, nondesert land, and snow/ice.

As Potter et al. (1988) point out, however, and as Taylor and Stowe (1984) recognized, the noon orbit of Nimbus-7 means that it views high latitudes at high solar zenith angles and low latitudes at low solar zenith angles, so that solar zenith angle variability is largely produced through latitudinal change. Thus, the Nimbus-7 measurements contain not only an albedo variation associated with solar zenith angle, but also a latitudinal change in planetary albedo due to latitudinal variations in surface albedo.

As a first step towards obtaining a more comprehensive understanding of the directional planetary albedo for various surface types in general, the present paper focuses upon a single clear-sky surface type—deserts—and we will essentially employ deserts in a tutorial role. Specifically, an atmospheric solar radiation model is employed to test for consistency between satellite-derived directional planetary albedos and surface bidirectional reflectance measurements. The model is further used to address issues such as the use of narrowband versus broadband instruments, the impact of desert aerosols upon the directional planetary albedo, and to interpret potential differences in the directional planetary albedo associated with different types of deserts.

2. Satellite-derived albedos

Listed below are sources of available satellite-derived directional planetary albedos over desert areas:

- Taylor and Stowe (1986); Nimbus-7
- Staylor and Suttles (1986); Nimbus-7
- Brooks (1987); GOES and METEOSAT.

* Dr. Inna Vulis passed away on 14 April 1988. She will be greatly missed by those of us who were fortunate enough to know her.

Corresponding author address: Prof. Robert D. Cess, Institute for Atmospheric Sciences, State University of New York at Stony Brook, Stony Brook, NY 11794-2300.

Variations of the planetary albedo $\alpha(\mu_0)$, as a function of μ_0 = cos(solar zenith angle) and determined from the above sources, are compared in Fig. 1 for clear-sky conditions, where the albedo has been normalized to its overhead-sun value, $\alpha(1)$.

The Taylor and Stowe (1986) results were obtained by first averaging the albedo over all desert areas and then normalizing to the overhead-sun value that, because of the noon orbit of Nimbus-7, is biased toward low-latitude desert regions. Both Staylor and Suttles (1986), and Brooks (1987), took advantage of the principle of reciprocity, which allows solar zenith angle and viewing zenith angle to be interchanged (Chandrasekhar 1960; Case and Zweifel 1967), such that normalized albedos were evaluated for individual deserts. The evaluation by Brooks refers to the Sahara Desert, while for Staylor and Suttles the evaluation as will shortly be discussed, is for a normalized albedo that is an average of the Sahara-Arabian, Saudi and Gibson Deserts.

The greatest disagreement in Fig. 1 pertains to Taylor and Stowe (1986), and this appears to be a consequence of the same problem as discussed in the Introduction. Specifically, different deserts, located at different latitudes, have different surface albedos, and consequently the resulting latitudinal variation in planetary albedo has been factored into the dependence of planetary albedo upon solar zenith angle.

Planetary albedos for three individual desert regions, as reported by Staylor and Suttles (1986), serve to illustrate this point. These are shown in Fig. 2, and clearly, there is a marked difference in planetary albedo for the three separate desert regions. Curiously, however, these three deserts produce nearly identical directional albedos, as is illustrated in Fig. 3. Taylor and Stowe (1986) first averaged the planetary albedo over all desert areas and then divided by the overhead-sun value, whereas the results of Staylor and Suttles suggest that this procedure should be reversed. It is by no means obvious, though, as to why the normalized albedos of Fig. 3 are in such close agreement, and we will later return to this issue.

The difference between the Staylor–Suttles and Brooks normalized albedos (Fig. 1) does not appear to have a simple explanation. One possibility is that Brooks (1987) employed a dataset that combines measurements made by an instrument having a very narrow spectral filter (GOES) with one having a somewhat broader filter (METEOSAT), and that this combination of filter functions is incompatible with the broadband Nimbus-7 measurements used by Staylor and Suttles (1986). Brooks, however, has summarized measurements, made by all three instruments, in terms of a reciprocity scatter plot (Staylor, 1985) that indeed suggests compatibility of these instruments, and we will later show that this compatibility is consistent with an atmospheric solar radiation model.

3. Surface albedo models

The agreement between the normalized albedos for different deserts (Fig. 3) suggests that an atmospheric solar radiation model, incorporating a directional surface albedo based upon measurements for one desert, would, in fact, be useful for comparison with a satellite-

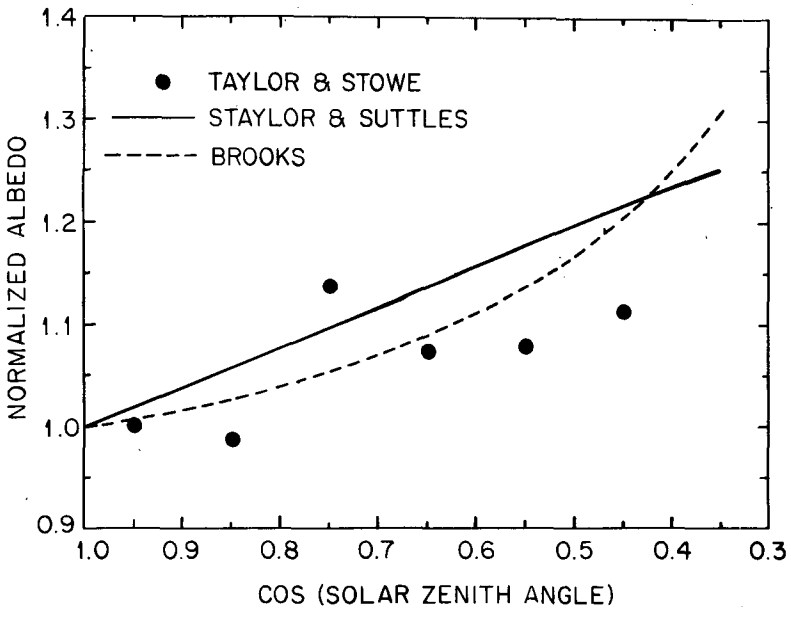

FIG. 1. Summary of directional planetary albedos for desert regions derived from Nimbus-7 data (Taylor and Stowe 1986; Staylor and Suttles 1986) and from combined GOES and METEOSAT data (Brooks 1987).

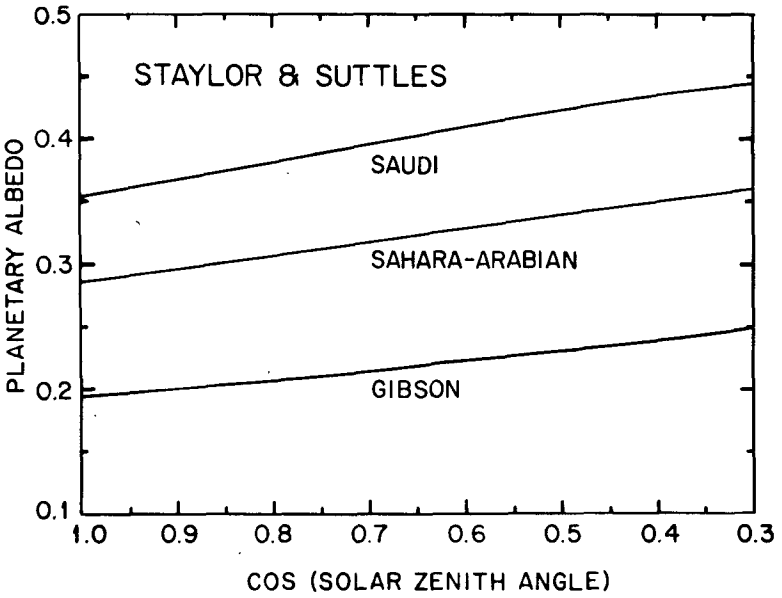

FIG. 2. Planetary albedos for three desert regions derived from Nimbus-7 data (Staylor and Suttles 1986).

derived directional planetary albedo for a different desert. The most comprehensive desert surface measurements are the bidirectional reflectance measurements made by Whitlock et al. (1987) for the Sonora Desert in Arizona. These measurements refer to three solar zenith angles (13°, 31°, and 57°), a broad range of viewing zenith and azimuth angles, and wavelengths of 0.40, 0.55, 0.65, 0.75 and 1.65 μm. The measurements were made from a helicopter at an altitude of 0.3 km, and a correction was made to account for the underlying atmosphere.

For the purpose of converting these bidirectional reflectance measurements to a directional surface albedo, we adopt a procedure due to Staylor (1985), which was subsequently employed by Staylor and Suttles (1986). By taking advantage of reciprocity between viewing

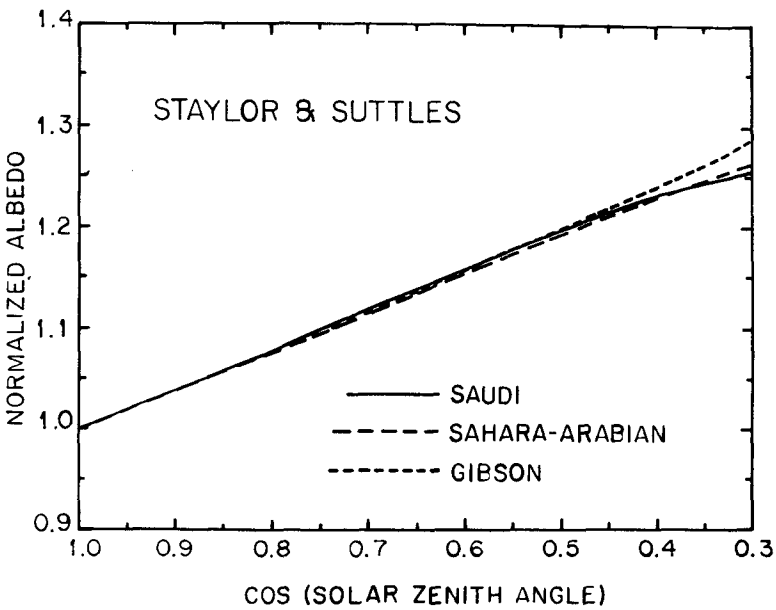

FIG. 3. Directional planetary albedos for three desert regions evaluated from the planetary albedos (Staylor and Suttles 1986) in Fig. 2.

zenith angle and solar zenith angle, this method, when applied to the Sonora Desert data, expands the number of "effective" solar zenith angles from 3 to 16, encompassing the entire range of viewing zenith angle (0° to 70°).

Letting μ = cos(viewing zenith angle) while ϕ denotes the azimuth angle, and recalling that μ_0 = cos(solar zenith angle), an azimuthally independent surface reflectance is defined as

$$\bar{R}(\mu, \mu_0) = (1/\pi) \int_0^{\pi} R(\mu, \mu_0, \phi) d\phi \qquad (1)$$

where $R(\mu, \mu_0, \phi)$ is the bidirectional reflectance. Following Barkstrom (1973), it has been shown (Staylor 1985; Staylor and Suttles 1986) that satellite-derived $\bar{R}(\mu, \mu_0)$ data may be correlated in terms of

$$X = \frac{\mu\mu_0}{\mu + \mu_0}, \quad y = \mu\mu_0 \bar{R}(\mu, \mu_0)$$

and this correlation is illustrated in Fig. 4 for the Sonora Desert surface and 0.55 μm. Also shown in Fig. 4 is a regression fit of the form

$$y = Ae^{NX}. \qquad (2)$$

For the present application, this was found to provide a better fit than the power-law expression adopted by Staylor (1985), and by Staylor and Suttles (1986). Table 1 summarizes the values of A and N as a function of wavelength. The directional albedo is, in turn, evaluated from

$$\alpha(\mu_0) = 2 \int_0^1 \bar{R}(\mu, \mu_0) \mu d\mu.$$

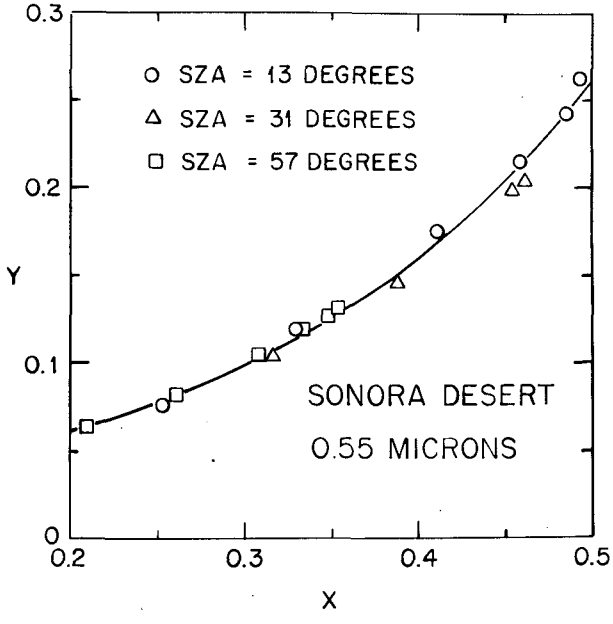

FIG. 4. Correlation of the directional reflectance of the Sonora Desert surface at 0.55 μm. The solid curve represents the regression fit given by Eq. (2).

TABLE 1. Values of the coefficients A and N in (2) for the Sonora Desert surface.

Wavelength (μm)	A	N
0.40	0.01502	4.013
0.55	0.02329	4.831
0.65	0.02865	5.106
0.75	0.03100	5.293
1.65	0.03571	5.427

As discussed by Staylor (1985), a scatter plot such as Fig. 4 serves the purpose of testing the consistency of a dataset. In the present context this is important, since it serves to assess the possible impact of desert aerosols upon the surface reflectance measurements. For example, such aerosols will produce a diffuse component to the surface insolation, and if this is significant it will degrade the correlation shown in Fig. 4. This correlation is applicable only for direct-beam radiation, since μ_0 characterizes solely the direct-beam contribution and not the diffuse component.

This fact is amply illustrated in Table 2, which shows a degradation of the correlation coefficient at 0.40 μm due to diffuse surface insolation resulting from Rayleigh scattering. The closeness of the correlation coefficient to unity at longer wavelengths, where Rayleigh scattering is significantly diminished, suggests that there is a minimal aerosol-induced diffuse component to the surface insolation.

Normalized surface albedos are summarized in Fig. 5 for the Sonora Desert, with exclusion of that at 0.40 μm for the reason explained above. Note the rather significant wavelength dependence. Here, and throughout the remainder of this paper, we restrict μ_0 to 0.35 or greater, since this coincides with the maximum viewing zenith angle (and through reciprocity the maximum solar zenith angle) of 70° for the surface reflectance data.

Returning to Fig. 4, it may be observed that the Staylor procedure is strongly weighted towards small solar zenith angles. In fact, results virtually identical to those of Fig. 5 are obtained by employing only data for a solar zenith angle of 13°. This is fortunate, since Whitlock et al. (1987) have additionally performed surface measurements for the Mohawk Valley, a small desert located to the north of the Sonora Desert, but only for a solar zenith angle of 21°.

TABLE 2. Correlation coefficients for the Staylor procedure as applied to the Sonora Desert surface.

Wavelength (μm)	Correlation coefficient
0.40	0.981
0.55	0.997
0.65	0.997
0.75	0.996
1.65	0.996

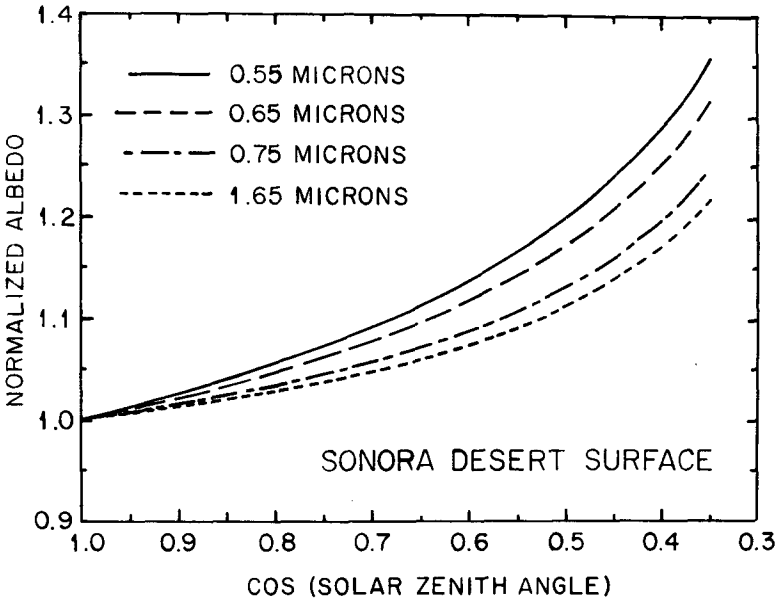

FIG. 5. Directional surface albedos for the Sonora Desert.

Employing this single solar zenith angle, consistent with our test calculation for the Sonora Desert, directional surface albedos for the Mohawk Valley are summarized in Fig. 6. Note the distinctly different dependence upon wavelength as opposed to the Sonora Desert (Fig. 5), and this appears to be due to differences in vegetation cover for the two deserts. The Sonora Desert is partially vegetated in a fairly uniform manner, whereas vegetation over the Mohawk Valley is much more sparse (Whitlock et al. 1987). The two deserts also exhibit differing overhead-sun albedos as is illustrated in Fig. 7. Here the "Sonora model" and the "Mohawk model" refer to interpolation and extrapolation, for use within the atmospheric solar radiation model described in section 5, of the overhead sun albedos shown in Fig. 7 that were evaluated from the surface radiance measurements.

The Sonora Desert data additionally serve as an

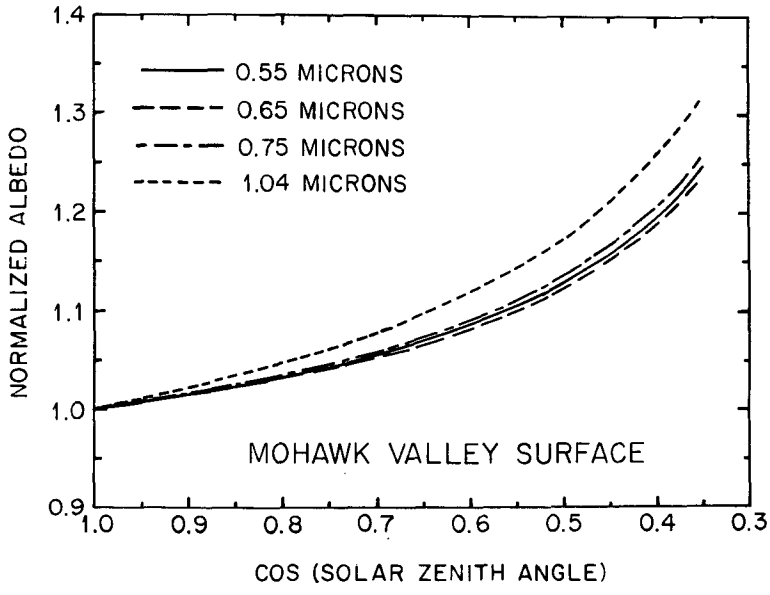

FIG. 6. As in Fig. 5, except for the Mohawk Valley.

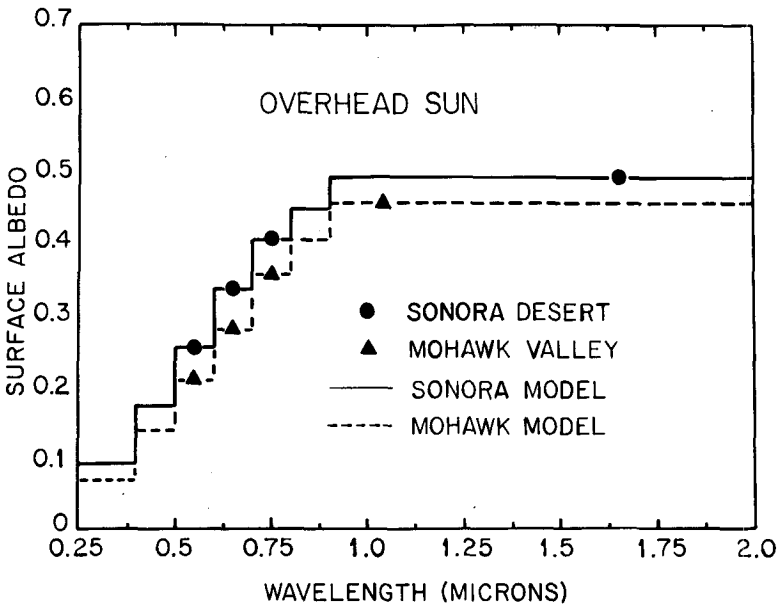

FIG. 7. Overhead-sun surface albedos for the Sonora Desert and the Mohawk Valley. The points and triangles are the overhead sun albedos as evaluated from the surface radiance measurements.

"educational" dataset for the purpose of investigating potential data processing techniques that might prove useful in dealing with top-of-the-atmosphere satellite data. For example, an alternate means of producing directional albedos from the Sonora bidirectional reflectance measurements utilizes an empirical reflectance model. Letting γ denote the scattering angle, where

$$\cos\gamma = [(1 - \mu^2)(1 - \mu_0^2)]^{1/2} \cos\phi - \mu\mu_0$$

the bidirectional reflectance measurements have been correlated by the regression fit

$$R(\mu, \mu_0, \phi) = 0.243 + 0.096z + 0.328z^2 + 0.117z^3 \tag{3}$$

where

$$z = \frac{\cos\gamma}{(\mu + \mu_0)^{1.15}}.$$

This fit is illustrated in Fig. 8 for the Sonora Desert and for the wavelength of 0.55 μm.

The interesting point here is that, in contrast to the Staylor procedure, this empirical radiance model is strongly weighted towards large solar zenith angles. For example, virtually the same result is obtained by employing the single solar zenith angle of 57°, as opposed to the Staylor procedure which essentially requires only the 13° solar zenith angle. Nevertheless, the two approaches produce comparable directional surface albedos, as is illustrated in Fig. 9 for 0.55 μm.

The surface albedo results summarized within Figs. 5, 6, 7 and 9 will subsequently be incorporated within atmospheric solar radiation models. For these models to be useful with respect to desert regions, they require a desert aerosol model, and this is described in the following section.

4. Desert aerosol model

For present purposes we adopt optical properties for desert aerosols from d'Almeida (1987), employing an extinction-coefficient weighted composite of his wind-carrying dust and sandstorm concentrations. Summarized in Table 3 are values of the asymmetry factor g, the single scattering albedo ω, and the ratio of aerosol optical depth τ to that at 0.55 μm, for the wavelength intervals of d'Almeida.

As pointed out by Longtin et al. (1988), d'Almeida (1987) has assumed the same optical constants for all modes of the size distribution, which probably underestimate the single scattering albedo, but as we illustrate in section 6, this seems to have minimal impact upon the directional planetary albedo. d'Almeida (1987) has conveniently summarized both daily and monthly mean values of aerosol optical depth at 0.5 μm for a number of desert stations in Africa, from which we choose for our nominal model, τ (0.55 μm) = 0.5, together with sensitivity studies that adopt τ (0.55 μm) = 0 and 1.0.

5. Atmospheric radiation models

The solar radiation model principally used within the present study is a delta-Eddington model. However, as discussed by Cess et al. (1981), any solar radiation

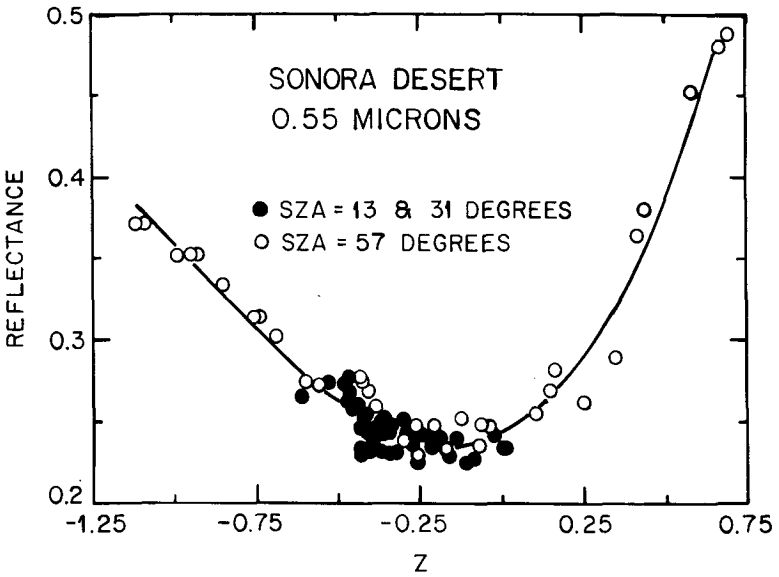

FIG. 8. Correlation of the azimuthally dependent directional reflectance of the Sonora Desert surface at 0.55 μm. The solid curve represents the regression fit given by Eq. (3).

model that is strictly a flux model, such as two-stream and delta-Eddington models, inherently violates reciprocity when employed in conjunction with a non-Lambertian surface. The reason is that flux models implicitly assume that solar radiation is diffusely reflected by the surface, which, through reciprocity, is inconsistent with the use of a surface albedo that is dependent upon solar zenith angle. The only way a non-Lambertian surface can produce diffuse reflection, while satisfying reciprocity, would be for the incident radiation to likewise diffuse. Cess et al. (1981) have illustrated that this is not a significant problem with respect to volcanic aerosols. In order to show that this is also the case for desert aerosols, we additionally employ, as did Cess et al. (1981), a doubling-adding model for comparison purposes. Both the delta-Eddington and doubling-adding models are described in subsections 5a, 5b, and 5c.

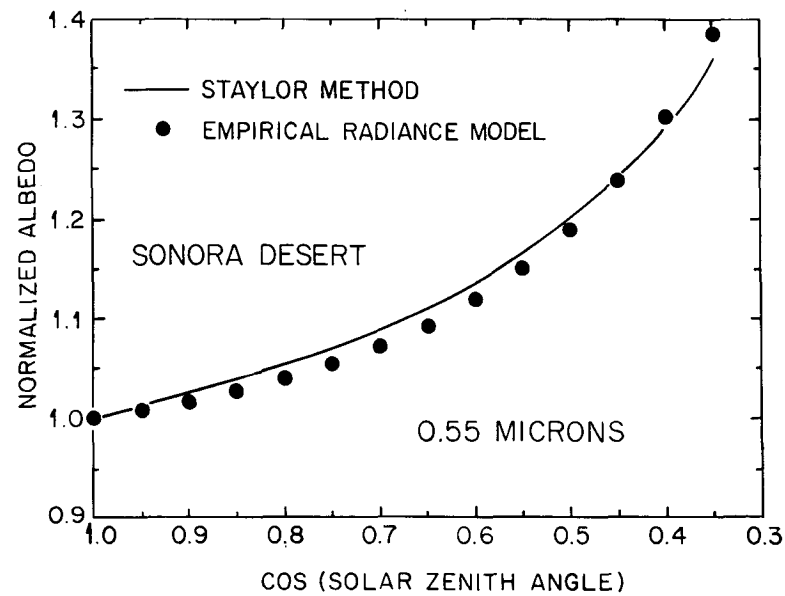

FIG. 9. Comparison of directional surface albedos for the Sonora Desert at 0.55 μm.

TABLE 3. Optical properties of the desert aerosol, where g denotes the asymmetry factor, ω is the single scattering albedo, and τ the aerosol optical depth.

Wavelength interval (μm)	g	ω	τ/τ (0.55 μm)
0.30–0.45	0.82	0.72	0.98
0.45–0.70	0.81	0.76	1.00
0.70–1.00	0.81	0.77	1.00
1.00–4.00	0.87	0.85	1.01

a. Delta-Eddington model

The delta-Eddington model is essentially that discussed by Cess et al. (1985), but with increased spectral resolution and modifications concerning gaseous absorbers. The spectral resolution, Rayleigh optical depth, and gaseous absorbers are summarized in Table 4. It should be noted that the spectral resolution of Table 4 is insufficient to account for the strong wavelength dependence of Rayleigh scattering, and thus the values of τ_R listed in Table 4 were determined by further subdivision of each interval and then evaluating a mean τ_R that reproduced the atmospheric Rayleigh reflectance for that interval. The solar spectral irradiance is taken from Thekaekara (1972).

Both the UV (0–0.31 μm) and visible (0.5–0.7 μm) ozone absorption parameterizations are from Lacis and Hansen (1974), renormalized from their full solar spectrum to the wavelength intervals of Table 4. Ozone absorption is assumed to occur above Rayleigh scattering. Absorption by the 0.72 and 0.81 μm H_2O bands was parameterized by a single exponential fit to the line-by-line calculations of Lee (1988). For H_2O absorption at wavelengths greater than 0.9 μm, the latter five terms of the six-term exponential sum fit presented by Somerville et al. (1974) were used. The first term in this sum fit represents absorption by H_2O at wavelengths less than 0.9 μm, and this has already been incorporated within the present model through our inclusion of the 0.72 and 0.81 μm bands. The desert aerosol is located within the model's lowest layer (800–1000 mb), while inclusion of atmospheric water vapor is as in Potter et al. (1988). They adopted GCM-generated water vapor mixing ratios for July at latitudes 42°S and 42°N, and they showed that the directional planetary albedo was the same for these two choices. July 42°N mixing ratios are employed in the present study.

b. Doubling-adding model

For present purposes we employ a doubling-adding model that incorporates both Rayleigh scattering and desert aerosols. The atmosphere is treated as a single homogeneous layer, which is equivalent to assuming that the desert aerosol is uniformly mixed within the atmosphere. While this is not the case for the real atmosphere, it is sufficient for the present goal of appraising the importance of the surface reciprocity inconsistency.

This one-layer model is a subset of the multilayer doubling-adding model developed by Lacis and Hansen (1974). The present version incorporates any arbitrary functional form of the surface bidirectional reflectance by utilizing a Fourier series expansion of the bidirectional reflectance in terms of azimuth angle. The computational procedure involves first employing a very thin homogeneous sublayer (optical depth = 10^{-20}), and then repetitively doubling this until the desired optical depth is achieved. The subsequent evaluation of the planetary albedo as a function of solar zenith angle is determined by performing numerical quadratures over viewing zenith and azimuth angles.

c. Model intercomparison

For the purpose of appraising the reciprocity inconsistency due to combining the delta-Eddington model with a non-Lambertian surface, we utilize the Sonora Desert at a wavelength of 0.55 μm where the largest departure from non-Lambertian behavior occurs (Fig. 5). The delta-Eddington model is correspondingly employed at this single wavelength, utilizing the directional surface albedo derived from the empirical radiance model (Fig. 9). This is then consistent with our use of the empirical radiance model, given by (3), within the doubling-adding model. Furthermore, to be consistent with the doubling-adding model, the desert aerosol is assumed to be uniformly mixed within the atmosphere, and ozone absorption is ignored, within this application of the delta-Eddington model. As previously mentioned, our purpose here is to test the reciprocity inconsistency, rather than replicate the actual atmosphere.

The percentage error in planetary albedo, for the delta-Eddington model relative to the doubling-adding model, and for the nominal aerosol optical depth of 0.5, is shown in Fig. 10 for both Lambertian and non-Lambertian surfaces. With the Lambertian surface the maximum error is 6.4%, which is typical of errors associated with the delta-Eddington approximation

TABLE 4. Spectral resolution, Rayleigh optical depth τ_R, and gaseous absorbers for the delta-Eddington model.

Spectral interval (μm)	τ_R	Gaseous absorber
0–0.31	7.065	O_3
0.31–0.4	0.630	—
0.4–0.4	0.226	—
0.5–0.6	0.099	O_3
0.6–0.7	0.050	O_3
0.7–0.8	0.028	H_2O (0.72 μm band)
0.8–0.9	0.017	H_2O (0.81 μm band)
>0.9	—	H_2O

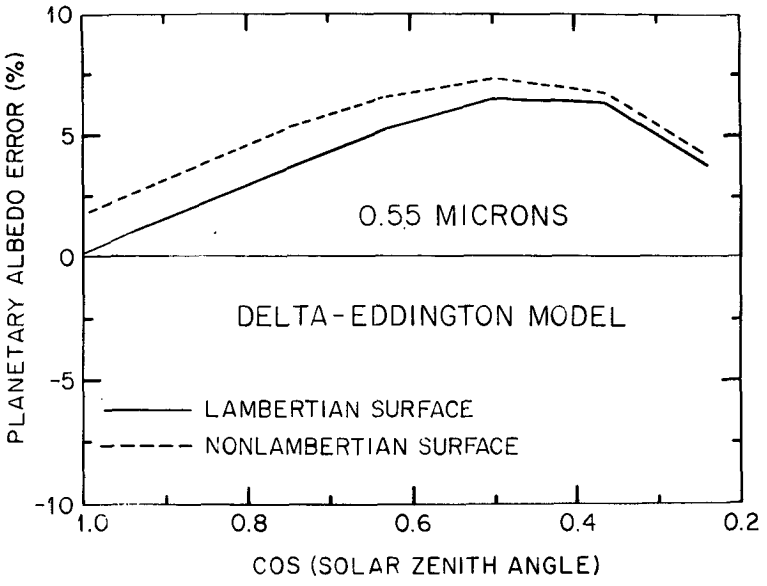

FIG. 10. Percentage errors in the planetary albedo as evaluated by the delta-Eddington model relative to the doubling-adding model.

(Coakley et al. 1983; King and Harshvardhan 1986). What is important here is that in comparing the non-Lambertian to Lambertian surface results, the error due to the reciprocity inconsistency is found to be less than 1.7%. Thus, this inconsistency, at least for the present application, is clearly not an issue.

6. Model simulations

In this section we employ the delta-Eddington model to address a number of issues related to understanding the directional planetary albedo for desert regions.

First, we return to the differences in directional surface albedo for the Sonora Desert (Fig. 5) versus the Mohawk Valley (Fig. 6). Directional planetary albedos, as evaluated from the delta-Eddington model and employing the surface albedo information summarized in Figs. 5–7, are presented in Fig. 11. The Mohawk Valley result exhibits a somewhat stronger dependence upon solar zenith angle than does that for the Sonora Desert, and the reason for this is rather subtle. For example, we also illustrate in Fig. 11 a model calculation that combines the Mohawk Valley directional surface albedo with the Sonora Desert overhead-sun albedo, and this shows that the different directional spectral surface albedos (Figs. 5 and 6) introduce a very minimal impact upon the directional planetary albedo.

Instead, the difference between the Sonora Desert and Mohawk Valley results is due to the different overhead-sun surface albedos (Fig. 7). The reason is that, by themselves, water vapor and aerosol absorption produce limb darkening, whereas Rayleigh and aerosol scattering result in limb brightening. The impact of atmospheric scattering is enhanced by a darker surface, however, whereas a darker surface diminishes the impact of atmospheric absorption. Thus, going from the Sonora Desert to the darker Mohawk Valley enhances atmospheric limb brightening while simultaneously decreasing atmospheric limb darkening, and this explains the differences shown in Fig. 11.

The above explanation raises an interesting point concerning the close agreement between the Saudi, Sahara-Arabian and Gibson directional albedos as shown in Fig. 3. Since, as previously discussed, the different deserts have significantly different surface albedos, one would not, from our Sonora Desert and Mohawk Valley comparison, expect such agreement. If this agreement is real, though, then it would seem to be due to the influence of the differing surface albedos being compensated for by the surfaces having *different* directional surface albedos. Clearly it would be advantageous if more extensive measurements of desert surface albedos were available.

An obvious source of uncertainty in attempting to model the directional planetary albedo refers to aerosol loading, and, as summarized by d'Almeida (1987), this is highly variable. To gain some insight into this uncertainty, we show in Fig. 12 the model's dependence upon aerosol optical depth, utilizing here the Sonora Desert surface albedo, and this suggests that the effect upon the directional albedo is rather modest. The impact upon the planetary albedo is substantial, however, with the overhead-sun albedo being reduced from 0.29 to 0.19 as the optical depth is increased from 0 to 1.0. We note that Brooks (1987) has observed seasonal variability in both the planetary and directional plan-

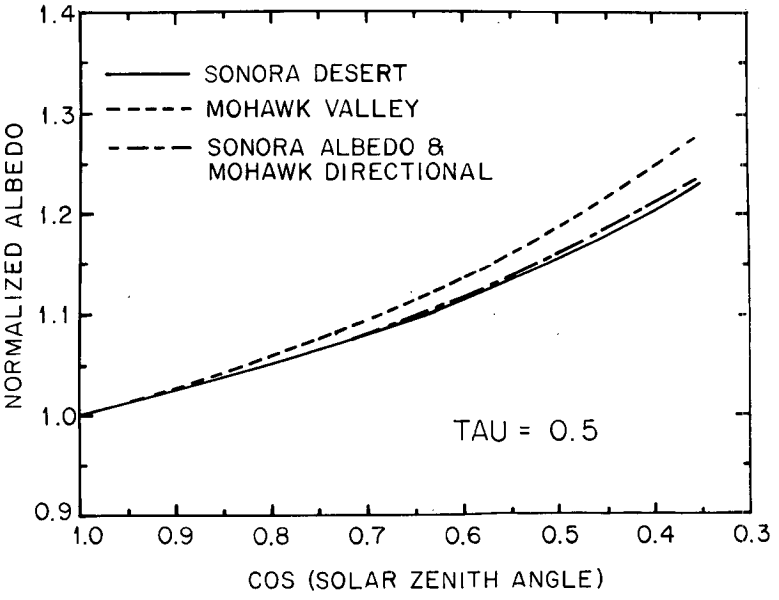

FIG. 11. Directional planetary albedos for the Sonora Desert and the Mohawk Valley as evaluated from the delta-Eddington model. Also shown is a model simulation utilizing the overhead-sun albedo for the Sonora Desert surface together with the directional surface albedo for the Mohawk Valley.

etary albedos, and a speculative suggestion is that this is due to seasonal variability in aerosol loading. Indeed, d'Almeida (1987) has shown substantial seasonal variability in aerosol optical depth for a number of locations in Africa.

A further source of model uncertainty refers to the optical properties of the aerosol. As we have previously mentioned, Longtin et al. (1988) have suggested that d'Almeida (1987) underestimated the single scattering albedo. For the purpose of a sensitivity study, we have replaced his values (Table 3) by $\omega = 0.9$. Modeled directional albedos, employing both this modified aerosol model and d'Almeida's model, are compared in Fig. 13, and the effect here is comparable to the TAU = 0

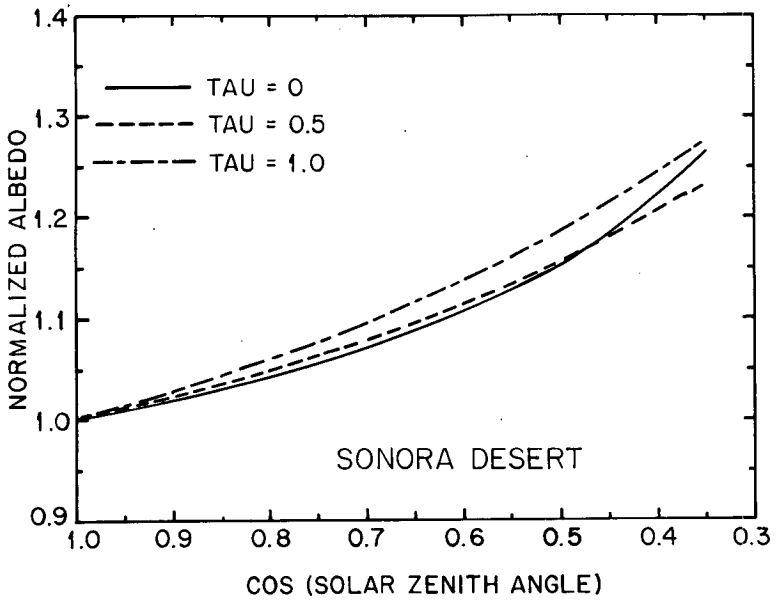

FIG. 12. The effect of aerosol optical depth, TAU, upon the directional planetary albedo for the Sonora Desert as evaluated from the delta-Eddington model.

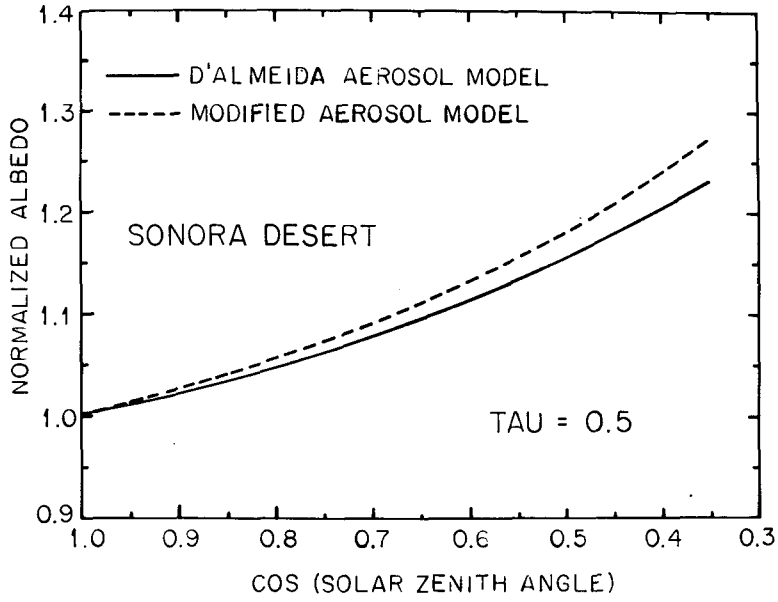

FIG. 13. The effect of different aerosol models upon the directional planetary albedo as evaluated from the delta-Eddington model and for the aerosol optical depth TAU = 0.5.

to TAU = 1.0 change in Fig. 12. Replacing the d'Almeida model by the modified aerosol model increased the overhead sun albedo from 0.233 to 0.264. Realistically, of course, there is no such thing as a "universal" desert aerosol model. As previously emphasized, optical properties of desert surfaces differ considerably from one desert to another, and since the surface is the primary source of the aerosol, the same should be true for desert aerosols.

A potential source of confusion, when intercomparing directional planetary albedos as derived from different satellite datasets, refers to the use of different instruments. As previously discussed, Staylor and Suttles (1986) employed broadband Nimbus-7 measurements, whereas Brooks combined narrowband GOES and METEOSAT measurements, with the former referring to a very narrow filter function, while that for the latter is somewhat broader. This raises the distinct possibility that directional albedos derived from GOES and METEOSAT data might not be representative of a broadband quantity.

There are several reasons for this being especially true for deserts. First, as already discussed, two important ingredients that govern the directional planetary albedo are limb brightening by Rayleigh scattering and limb darkening due to water vapor absorption. Both of these effects occur outside of the GOES filter function, and they are only partially contained within the METEOSAT filter function. A further limitation of the narrowband GOES and METEOSAT instruments is that they miss much of the wavelength dependence of the directional surface albedo (Figs. 5 and 6), but as we have previously mentioned, Brooks (1987) has shown compatibility of GOES, METEOSAT and Nimbus-7 data in terms of a scatter plot similar to that of Fig. 4.

To additionally address this issue, we have incorporated a square-wave filter function into the delta-Eddington model, employing a wavelength interval of 0.55–0.75 μm to simulate GOES, and 0.45–0.90 μm as an analog to METEOSAT. The modeled directional albedos are compared, using the Sonora Desert model, in Figs. 14 and 15 for, respectively, aerosol optical depths of 0 and 0.5. Given the aforementioned pitfalls associated with using a narrowband instrument to obtain broad-band directional albedos over deserts, the agreement shown in Figs. 14 and 15 is quite remarkable. Indeed, this agreement extends to the Mohawk Valley, as shown in Fig. 16, despite the fact that this desert has a different wavelength dependence of its surface albedo, and by being darker than the Sonora Desert, as previously discussed, it has differing limb brightening and limb darkening contributions. Clearly the agreement shown in Figs. 14–16 is due to numerous compensatory processes, but recall that this agreement is consistent with the data intercomparison of Brooks (1987).

The overall picture presented by the comparisons shown in Figs. 11–16 is that there are many sources of uncertainty associated with modeling the directional planetary albedo for desert regions. Individually, these uncertainties appear modest, although collectively they might be significant. Presented in Fig. 17 is a summary of the Sonora Desert and Mohawk Valley models together with the satellite-derived results of Staylor and Suttles (1986) and of Brooks (1987). Given the many

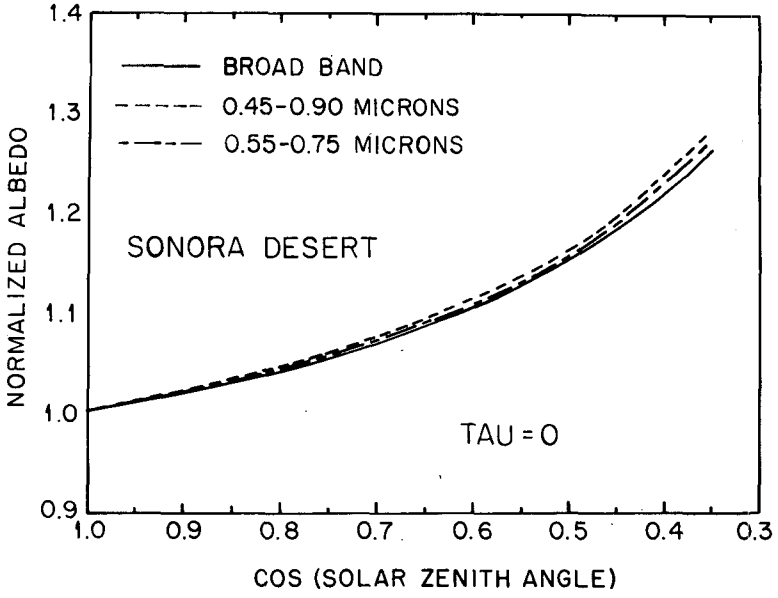

FIG. 14. Comparison of narrowband versus broadband evaluations of the directional planetary albedo using the delta-Eddington model, for the aerosol optical depth TAU = 0, and for the Sonora Desert.

sources of uncertainty, the agreement shown in Fig. 17 is quite respectable.

One final point. Summarized within Fig. 18 is a sequence of simulations utilizing TAU = 0 and 0.5, employing the Sonora Desert surface albedo (non-Lambertian), and additionally adopting the assumption of a Lambertian surface in which the directional surface albedo is replaced by the spherical albedo. This quantity is defined as

$$\bar{\alpha} = 2\int_0^1 \alpha(\mu_0)\mu_0 d\mu_0$$

and it represents averaging over a sphere while holding the position of the sun fixed. Alternatively, $\bar{\alpha}$ is easily shown to also be the average albedo for diffuse incident radiation. In this context, it denotes the equivalent Lambertian albedo, since reflected radiation from a Lambertian surface is diffuse as is that from a non-

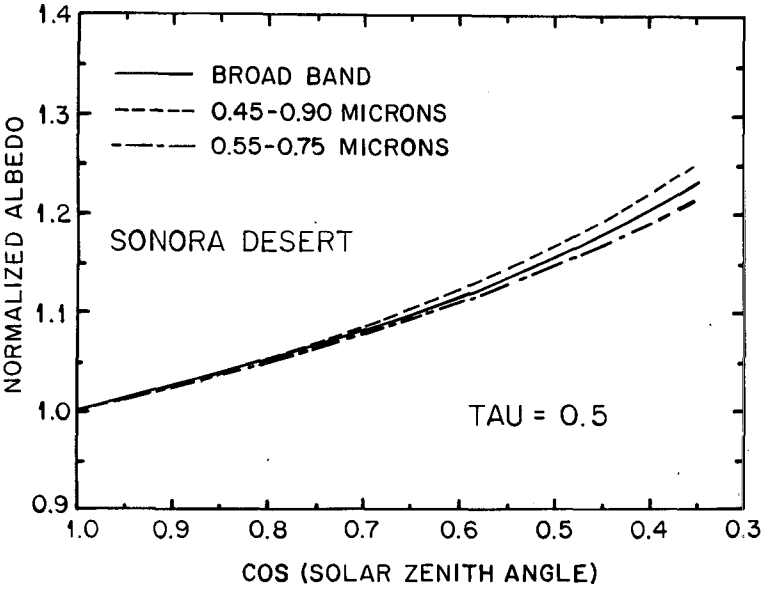

FIG. 15. As in Fig. 14, but for the aerosol optical depth TAU = 0.5.

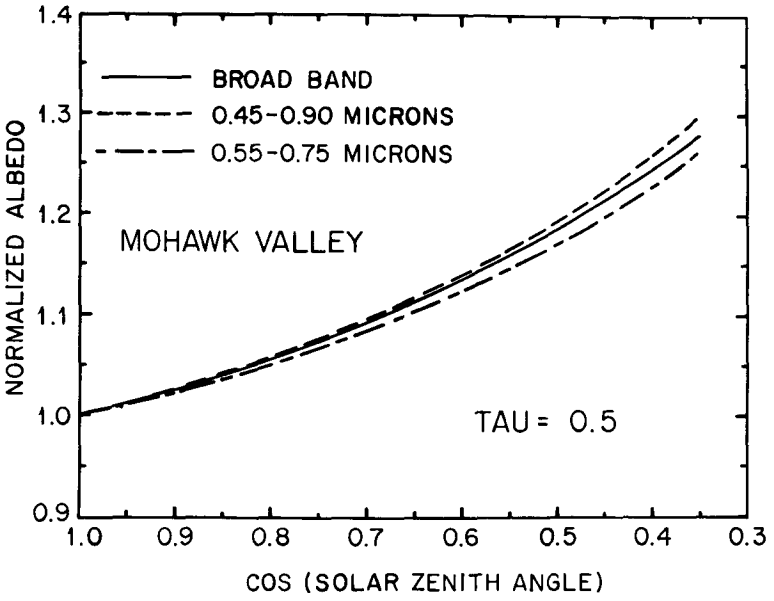

FIG. 16. As in Fig. 15, but for the Mohawk Valley.

Lambertian surface when the incident radiation is diffuse. There are two points to note from Fig. 18. First, the directional planetary albedo is clearly dominated by the directional surface albedo; and second, inclusion of the directional surface albedo substantially moderates the aerosol impact upon the directional planetary albedo.

7. Concluding remarks

The present study has focused upon a single land surface type, deserts, as a means of obtaining a more complete understanding of satellite-derived directional planetary albedos. It is emphasized, for example, that in evaluating the directional planetary albedo from

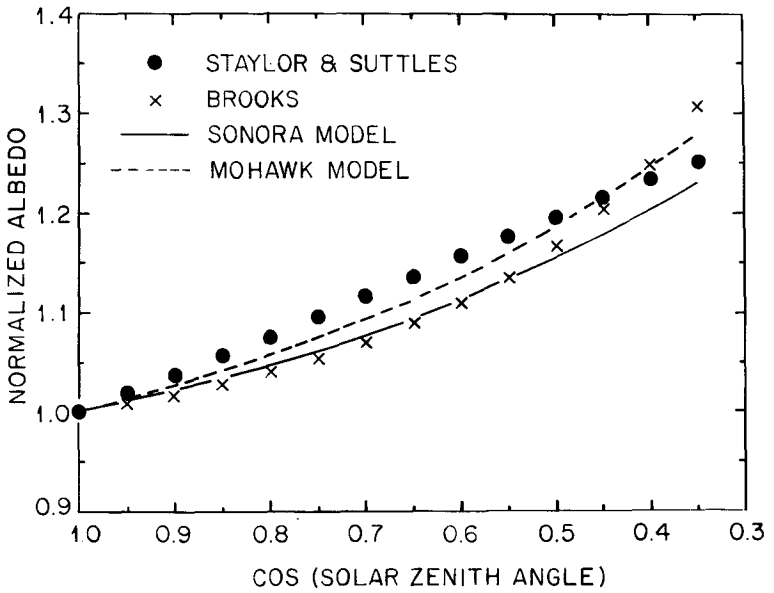

FIG. 17. Comparison of the directional planetary albedos as determined from the delta-Eddington model for the Sonora Desert and Mohawk Valley, from Nimbus-7 data (Staylor and Suttles 1986), and from GOES and METEOSAT data (Brooks 1987).

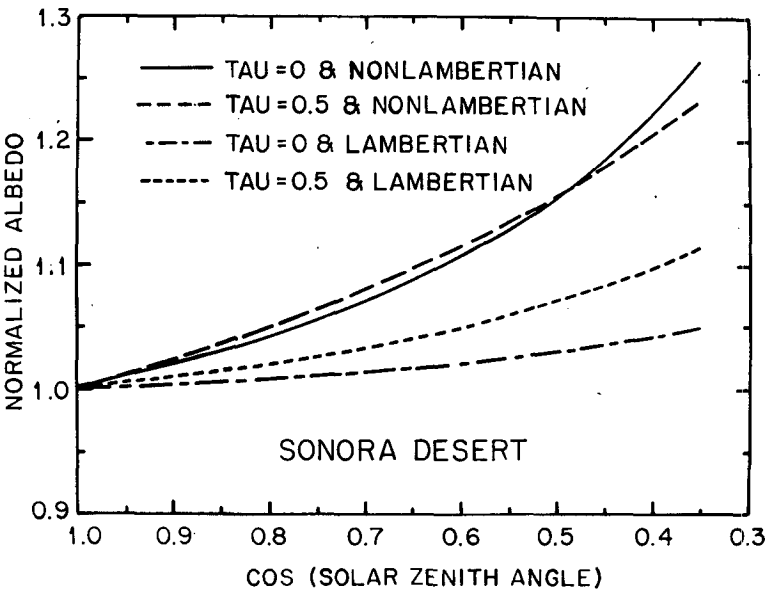

FIG. 18. Comparison of directional planetary albedos for the aerosol optical depths TAU = 0 and 1.0, and with and without the assumption of a Lambertian surface.

satellite data, care must be exercised so not to factor in latitudinal variations of planetary albedo.

The present study further employed an atmospheric solar radiation model, in conjunction with surface bidirectional reflectance measurements, to address a number of issues related to our understanding of directional planetary albedos. Of particular note is the suggestion that measurements made by narrowband instruments, such as GOES, METEOSAT and AVHRR, seem to replicate broadband measurements, a conclusion that is consistent with an observational study by Brooks (1987). As we have emphasized, however, this compatibility is due to several compensatory effects, and thus this conclusion should not be extrapolated to regions other than deserts without further investigation.

The atmospheric solar radiation model further produced directional planetary albedos that were consistent with selected, and understood, satellite measurements. This, in turn, indicates consistency between surface and top-of-the-atmosphere measurements, since surface measurements were used in formulating the model's lower boundary conditions. The model results also illustrate that the directional planetary albedo is dominated by the directional surface albedo, although surface brightness is a second factor since it influences atmospheric limb brightening and darkening processes.

Acknowledgments. We thank Dimitri L. Vulis for his assistance, and we benefited from useful discussions with D. R. Brooks, J. A. Coakley, Jr., E. F. Harrison, A. A. Lacis, W. B. Rossow, E. P. Shettle, J. T. Suttles and L. D. Travis. This work was supported by NSF Grant ATM8515310 to SUNY Stony Brook, and by NASA through cooperative Agreement NCC5-29 to Columbia University.

REFERENCES

Barkstrom, B. R., 1973: A comparison of the Minneart reflectance law and the reflectance from a nonconservative isotropic scattering atmosphere. *J. Geophys. Res.*, **78,** 6370–6372.

Brooks, D. R., 1987: Parameterized angular models for interpreting satellite-based measurements of shortwave and longwave radiances over deserts. Ph.D. thesis, University of London, Imperial College of Science and Technology, 313 pp.

Case, K. M., and P. F. Zweifel, 1967: *Linear Transport Theory,* Addison-Wesley.

Cess, R. D., J. A. Coakley, Jr. and P. M. Kolesnikov, 1981: Stratospheric volcanic aerosols: A model study of interactive influences upon solar radiation. *Tellus,* **33,** 444–452.

——, G. L. Potter, S. J. Ghan and W. L. Gates, 1985: The climatic effects of large injections of atmospheric smoke and dust: A study of climate feedback mechanisms with one- and three-dimensional climate models. *J. Geophys. Res.*, **90,** 12,937–12,950.

Chandrasekhar, S., 1960: *Radiative Transfer,* Dover.

Coakley, J. A., Jr., R. D. Cess and F. B. Yurevich, 1983: The effect of tropospheric aerosols on the earth's radiation budget: A parameterization for climate models. *J. Atmos. Sci.*, **40,** 116–138.

d'Almeida, G. A., 1987: On the variability of desert aerosol radiative characteristics. *J. Geophys. Res.*, **92,** 3017–3026.

King, M. D., and Harshvardhan, 1986: Comparative accuracy of selected multiple scattering approximations. *J. Atmos. Sci.*, **43,** 784–801.

Lacis, A. A., and J. E. Hansen, 1974: A parameterization for the absorption of solar radiation in the earth's atmosphere. *J. Atmos. Sci.*, **31,** 118–133.

Lee, J. N., 1988: Band absorptances of the near-infrared water vapor bands. M.S. thesis, State University of New York at Stony Brook.

Longtin, D. R., E. P. Shettle, J. R. Hummel and J. D. Pryce, 1988: A desert aerosol model for radiative transfer studies. *Aerosols and Climate.* P. V. Hobbs and M. P. McCormick, Eds. A. Deepak Publ.

Potter, G. L., R. D. Cess, P. Minnis, E. F. Harrison and V. Ramanathan, 1988: Diurnal variability of the planetary albedo: An appraisal with satellite measurements and general circulation models. *J. Climate,* **1,** 233–239.

Somerville, R. C. J., P. H. Stone, M. Halem, J. E. Hansen, J. S. Hogan, L. M. Druyan, G. Russel, A. A. Lacis, W. J. Quirk and J. Tenenbaum, 1974: The GISS model of the global atmosphere. *J. Atmos. Sci.,* **31,** 84–117.

Staylor, W. F., 1985: Reflection and emission models for clouds derived from Nimbus-7 ERB scanner measurements. *J. Geophys. Res.,* **90,** 8075–8079.

——, and J. T. Suttles, 1986: Reflection and emission models for deserts derived from Nimbus-7 ERB scanner measurements. *J. Climate Appl. Meteor.,* **25,** 196–202.

Taylor, V. R., and L. L. Stowe, 1984: Reflectance characteristics of uniform earth and cloud surfaces derived from Nimbus-7 ERB. *J. Geophys. Res.,* **90,** 4987–4996.

——, and ——, 1986: Revised reflectance and emission models from Nimbus-7 ERB data. Extended Abstracts, *Sixth Conf. on Atmospheric Radiation,* Amer. Meteor. Soc., J19–J22.

Thekaekara, M. P., 1972: Solar energy outside the earth's atmosphere. *Solar Energy,* **14,** 109–127.

Whitlock, C. H., G. C. Purgold and S. R. LeCroy, 1987: Surface bidirectional reflectance properties of two Southwestern Arizona deserts for wavelengths between 0.4 and 2.2 micrometers. NASA Tech. Pap. 2643, 44 pp. [Available from National Aeronautics and Space Administration, Code NTT-4, Washington, DC 20546-0001.]